processes

MDPI

Article

Cenozoic Subsidence History of the Northern South China Sea: Examples from the Qiongdongnan and Yinggehai Basins

Ming Ma [1], Jiafu Qi [2,*], Jinshan Ma [3], Heng Peng [4], Linlin Lei [5], Qian Song [1], Qing Zhang [1] and Mengen Bai [1]

1 Department of Geological Engineering, Qinghai University, Xining 810016, China; maming1002@126.com (M.M.)
2 State Key Laboratory of Petroleum Resource and Prospecting, College of Geosciences, China University of Petroleum, Beijing 102249, China
3 Xining Land Surveying and Planning Research Institute, Xining 810008, China
4 Department of Geology, Northwest University, Xi'an 710077, China
5 Research Institute of Logging Application, China Petroleum Logging Co., Ltd., Xi'an 710077, China
* Correspondence: qijiafu@cup.edu.cn

Abstract: The Qiongdongnan and Yinggehai Basins are important petroliferous basins. To study the Cenozoic subsidence characteristics of these two basins, their controlling factors, and their implications, we studied the basins' subsidence characteristics via one-dimensional, two-dimensional, and holistic subsidence. Then, we compared the basins' subsidence characteristics based on the evolution of several particular geological processes that occurred in the South China Sea (SCS) and adjacent areas. The results indicated that the change in the holistic subsidence of both basins occurred episodically. In addition, the subsidence in these two basins differed, including their subsidence rates, the migration of the depocenters, and the changes in the holistic subsidence. The dynamic differences between the two basins were the main factors controlling the differences in the subsidence in the two basins. In the Qiongdongnan Basin, the subsidence characteristics were primarily controlled by the mantle material flowing under the South China Block in the Eocene and the spreading of the SCS from the Oligocene to the Miocene. In the Yinggehai Basin, the subsidence characteristics were primarily controlled by the coupling between the uplift of the Tibetan Plateau and the strike-slip motion of the Red River Fault before the Early Miocene and by only the effect of the strike-slip motion of the Red River Fault from the Middle Miocene to the Late Miocene. Since the Pliocene, the subsidence characteristics of both basins have been principally controlled by the dextral strike-slip motion of the Red River Fault. The major faults contributed to the spaciotemporal variations in the subsidence within each basin.

Keywords: Qiongdongnan basin; Yinggehai basin; subsidence characteristics; variations; controlling factors

check for updates

Citation: Ma, M.; Qi, J.; Ma, J.; Peng, H.; Lei, L.; Song, Q.; Zhang, Q.; Bai, M. Cenozoic Subsidence History of the Northern South China Sea: Examples from the Qiongdongnan and Yinggehai Basins. *Processes* **2023**, *11*, 956. https://doi.org/10.3390/pr11030956

Academic Editors: Linhua Pan, Yushi Zou, Jie Wang, Minghui Li, Wei Feng and Lufeng Zhang

Received: 31 December 2022
Revised: 13 March 2023
Accepted: 16 March 2023
Published: 21 March 2023

1. Introduction

The South China Sea and the adjacent areas are characterized by complicated and diverse geological phenomena and are surrounded by the Indian, Eurasian, and Pacific plates. Thus, these areas are also referred to as a natural geological laboratory [1]. Regarding the formation mechanism and the dynamic processes of the evolution of the SCS and the adjacent areas, various dynamic models have been proposed by researchers around the world based regarding different methods, including the back-arc-spreading model [2], the collision-extrusion model [3,4], the mantle-upwelling model [5,6], and the expanding-continental-margin model [7]. However, there are still some conflicts among these models, and each model has limitations [8] Even for the same model, discrepancies exist between different studies. The Qiongdongnan Basin (QDNB) and the Yinggehai Basin (YGHB), located in the northern continental margin of the SCS, are two important petroliferous basins. However, the tectonic locations of these two basins are particularly specific, and the sedimentary stratigraphy and the structures of these two basins are significantly different. In addition, several particular geological processes, such as the uplift of the Tibetan Plateau, the strike-slip motion of the Red River Fault, and the expansion of the SCS during the Cenozoic period, have dramatically affected the subsidence, filling, and evolution of these two basins. However, the role of each geological process in the basins' evolutions is still not clear. In addition, the geodynamics of the basins are poorly understood and controversial.

A basin's subsidence history is the reestablishment of the basin's tectonic and sedimentary evolution, and it records the significant geological events and reflects the basin's evolution [9]. Conversely, the characteristics of a basin's subsidence are fundamentally controlled by the basin's dynamics [10]. In view of this, in this study, the similarities and the differences in the Cenozoic subsidence characteristics of the two basins were investigated via comparative analysis, and then, the subsidence features of the two basins were, as compared to the geological processes that occurred in the SCS and its adjacent areas to ascertain the main factors controlling the mechanisms of the subsidence found in these two basins. The results of this study provide important evidence for the reconstruction of the geodynamic processes as well as important theoretical guidance for the deployments of oil-and-gas exploration in these two basins [11–13].

2. Geological Setting

The QDNB and the YGHB are located in the northern continental margin of the SCS and are surrounded by the Indian, Eurasian, and Pacific Plates. They are adjacent basins but have significantly different formation mechanism [14]. The QDNB, located at the intersection of the northern SCS margin and the Red River Fault Zone, is NE trending and consists of three major tectonic units from northwest to southeast [15]: the northern depression, the central uplift, and the central depression. The structural framework of the QDNB is characterized by alternating depressions and uplifts (Figure 1). The YGHB is diamond-shaped, trends NW, and consists of three major tectonic units: the Yingdong slope; a central depression composed of the Yinggehai sag, Henei sag, and Lingao rise; and the Yingxi slope (Figure 1). The evolution of the QDNB and the YGHB can be divided into two stages as a whole: a rifting stage during the Paleogene period and a post-rifting stage from the Neogene to the Quaternary period, which can be further divided into depression and thermal subsidence stages [16,17] (Figure 2).

The strata in the QDNB and the YGHB have been studied in detail, except for the Paleocene and Eocene strata, which have not been sampled or assigned specific formation names (Figure 2). The Paleocene strata primarily consist of volcanic rocks in these two basins, but the difference is that a small amount of limestone was deposited in the YGHB. The Eocene strata primarily consist of lacustrine and alluvial-facies conglomerate, sandstone, and mudstone. The sediments of the Lower Oligocene Yacheng Formation, including the fluvial, lacustrine, swamp, and fan-delta facies, are finer grained than those of the previous period and consist of mudstone, sandstone, and siltstone. The difference between these two basins is that a coal seam developed in the QDNB, while shale developed in the YGHB. The upper Oligocene Lingshui Formation consists of more fine-grained sediments, including interbedded siltstone and mudstone, because the water depth increased, and the sedimentary environment changed into delta and littoral facies. From the Early Miocene to the end of the Middle Miocene, when the Sanya and Meishan Formations were deposited, the sedimentary characteristics were different in the two basins. The sediments in the QDNB mostly consisted of interbedded siltstone and mudstone under the shallow platform and littoral facies. However, most sediments in the YGHB are mudstone, which developed under the littoral-shallow facies. From the Late Miocene until the present, i.e., the deposition time of the Huangliu–Ledong Formations, thick mudstone and thin siltstone formed in the bathyal facies in the QDNB, whereas in the YGHB, the proportion of siltstone is higher [17].

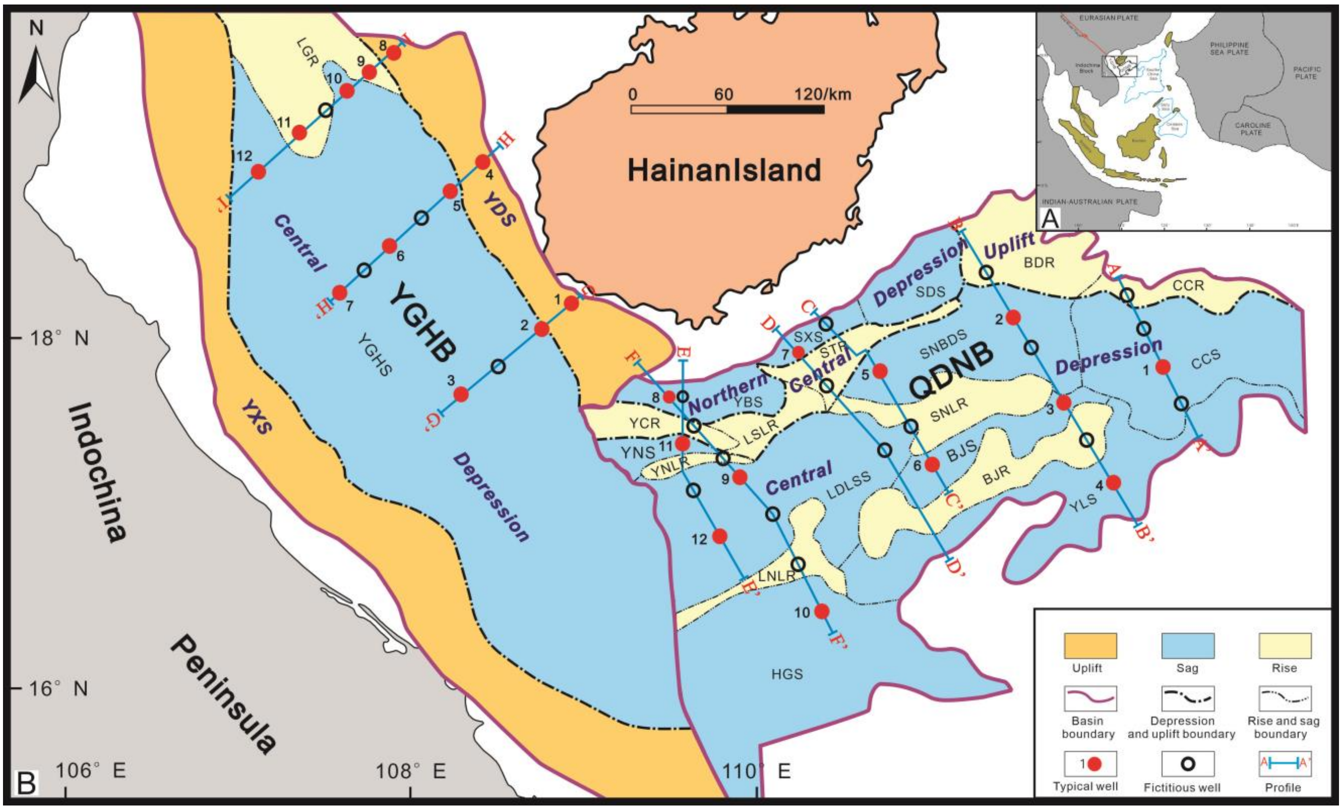

Figure 1. Map showing the tectonic units in the Qiongdongnan and Yinggehai Basins. YGHB, Yinggehai Basin; QDNB, Qiongdongnan Basin; YBS, Yabei sag; SXS, Songxi sag; SDS, Songdong sag; YNS, Yanan sag; SNBDS, Songnanbaodao sag; LDLSS, Ledonglingshui sag; BJS, Beijiao sag; CCS, Changchang sag; YLS, Yongle sag; HGS, Huangguang sag; YGHS, Yinggehai sag; YCR, Yacheng rise; LSLR, Lingshui low rise; YNLR, Yanan low rise; STR, Songtao rise; BDR, Baodao rise; CCR, Changchang rise; SNLR, Songnan low rise; LNLR, Lingnan low rise; BJR, Beijiao rise; LGR, Linggao rise. The locations of the wells and seismic profiles are also shown (modified after Shi et al. [18], Zhu et al. [19]).

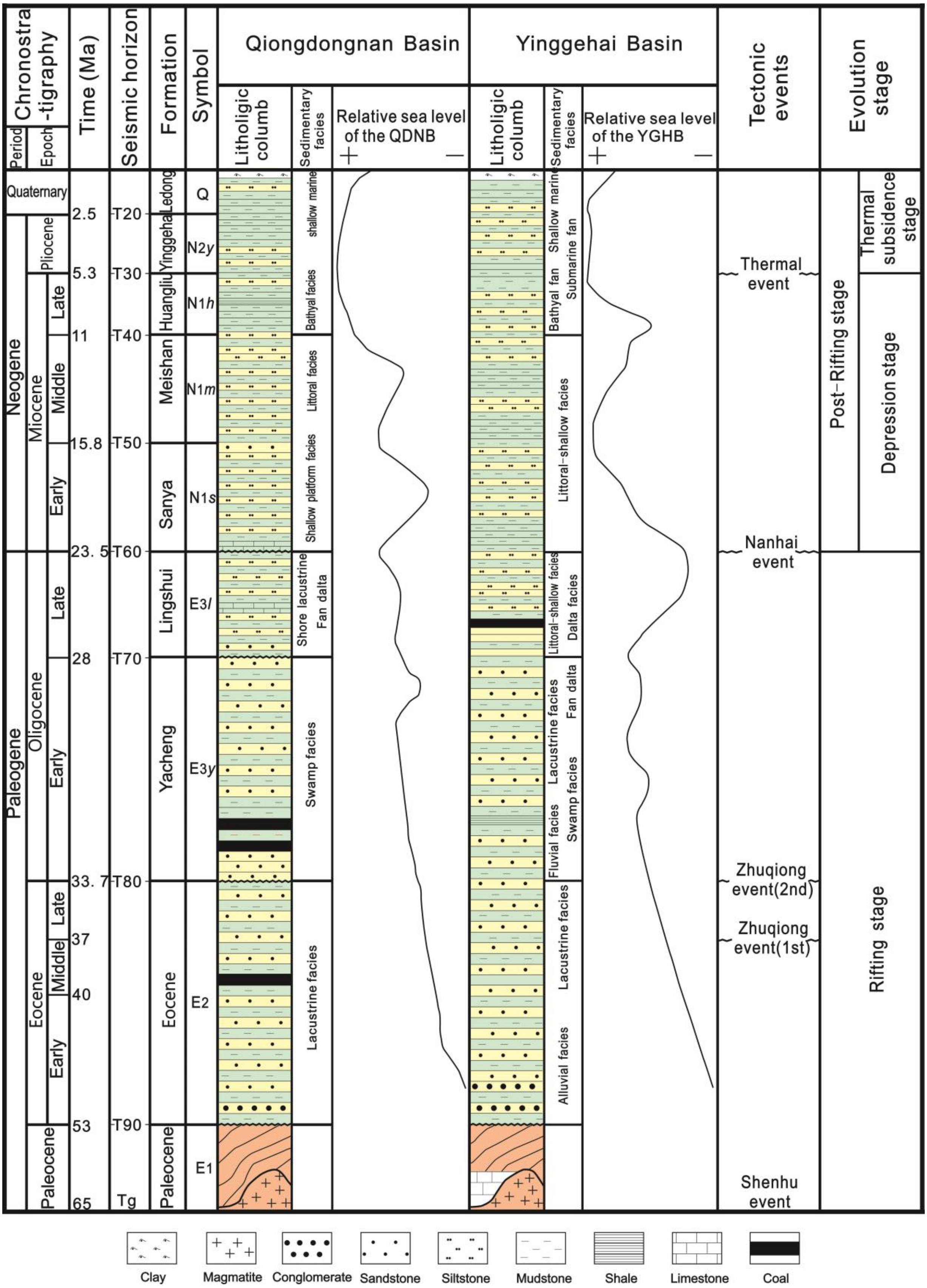

Figure 2. Simplified stratigraphic columns for the QDNB and the YGHB (modified after Zhu et al. [19], All China Commission of Stratigraphy [20], Wang et al. [21], Chen et al. [22], Liu et al. [23]).

3. Data and Methods

3.1. Data

Due to high acquisition costs, the well and seismic data in the QDNB and the YGHB are limited, and most of the early data are fragmentary in terms of the data needed to study subsidence, such as the lithology data. In this study, we chose three and six interpreted and most recently acquired seismic profiles for the analyses of the YGHB and QDNB, respectively. This effectively reduced the uncertainty and ensured the results were more reliable. The number of drilling wells was relatively small in the study area, as compared to the area of the two basins and the requirements of such a study. Therefore, several fictitious wells were created. To create this kind of well, the drilling wells were correlated with the seismic data first. Next, we chose several locations for the fictitious wells near the drilling wells on the seismic profiles for the calculations and analysis. Twenty-eight wells in QDNB and sixteen wells in the YGHB were selected to calculate and analyze their subsidence history (Figure 1). Most of the units were distributed by fictitious wells as soon as possible.

3.2. Method and Parameters

3.2.1. Methods

We analyzed the basin subsidence at three levels, i.e., the subsidence of single wells (1D), the subsidence along the profile (2D), and the subsidence of the entire basin. As for the subsidence calculation process, we synthesized and improved the traditional back-stripping method. The details are provided below.

The total subsidence (STT) of the basin could be divided into four components, namely, the tectonic subsidence induced by tectonism (ST), the loading subsidence caused by the sediments (D), the loading subsidence induced by sea-level changes (D(ΔL)), and the retroaction induced by the lithosphere (DT), which could be ignored in extensional basins [18,24]. Thus, the abovementioned relationships could be expressed mathematically as follows:

$$\text{STT} = \text{ST} + \text{D} + \text{D}(\Delta\text{L}). \tag{1}$$

The total subsidence (STT) could be expressed as follows:

$$\text{STT} = \text{Hs} + \text{Hw} + \Delta\text{L}, \tag{2}$$

where Hs is the de-compacted stratum thickness, which could be obtained using the Authy equation [25]; Hw is the paleo-water depth; and ΔL is the value of the eustatic sea-level change. Hw and ΔL could be acquired in several ways, which is introduced in detail in a subsequent section.

The loading subsidence caused by the sediments (D) and the loading subsidence induced by sea-level change (D(ΔL)) could be acquired based on the Airy isostasy [26], as follows:

$$\text{D} = \text{Hs} \times (\varrho\text{s} - \varrho\text{w})/(\varrho\text{m} - \varrho\text{w}), \tag{3}$$

$$\text{D}(\Delta\text{L}) = \Delta\text{L} \times \varrho\text{w}/(\varrho\text{m} - \varrho\text{w}), \tag{4}$$

where ϱs, ϱm, and ϱw are the densities of the mean sediments, mantle, and water, respectively. Finally, we could easily acquire the tectonic subsidence (ST) using Equation (1).

The total subsidence and tectonic subsidence could be acquired simultaneously by using this technique. In addition, several controversial problems could be avoided by using this method, for example, the water-loaded basin subsidence and the uncertainty of the parameters in the tectonic subsidence calculation [27].

The calculations were conducted using MATLAB (R2014a) with a precision set at 10^{-5}; Excel software for further data processing and mapping; and finally, CorelDRAW software for map beautification.

3.2.2. Parameters

Many parameters were involved in the subsidence calculations and analysis, and every parameter had to be analyzed and processed scientifically and reasonably.

- Dates of strata boundaries: First, we identified the different degrees of the chronostratigraphic units and rock stratigraphic units in the seismic and well profiles [19]. Then, we determined the age of every chronostratigraphic unit's boundary after chronostratigraphic correlation and constructed a chronostratigraphic framework [20,21]. We also determined the ages of each rock stratigraphic unit's boundaries after the rock stratigraphic correlation and analysis of the biological fossils [22,23]. Finally, the stratigraphic columns of the basins were constructed to study the sedimentology and tectonics of the basin (Figure 2).
- Porosity, density, and compaction coefficient: According to the basin's stratigraphy, we analyzed the lithology and proportions of each component of each formation. Based on the results, the density of each formation was calculated by averaging their weighted components, which ensured the credibility of the results [17]. The densities of the mantle and water were 3330 kg/m^3 and 1000 kg/m^3, respectively [28]. For the surface porosity and compaction coefficient, previously published results on the subsidence in the QDNB and the YGHB were directly adopted, and these only considered the sandstone and mudstone while ignoring the other components of the strata in the North Sea Basins [29]. Furthermore, the sedimentary and diagenetic environments of the QDNB and the YGHB are also different from their counterparts in the North Sea Basins. The differences between the two study areas inevitably induced errors. To reduce these errors as much as possible, we acquired the surface porosity and compaction coefficient in the same way as the density. The surface porosity and compaction coefficient of each lithology are listed in Table 1.

Table 1. Surface coefficient of compaction, surface porosity, and density of different lithologies in a normal environment (according to Gao et al. [24]).

Lithology	Surface Coefficient of Compaction (km^{-1})	Surface Porosity (%)	Density (kg/m^3)
Mudstone	0.51	0.63	2720
Sandy mudstone	0.39	0.56	2680
Sandstone	0.27	0.49	2650
Conglomerate	0.22	0.46	2640

- Paleo-water depth and eustatic sea-level change: There are many ways to estimate the paleo-water depth, including paleontology, sedimentary facies analysis, geochemical indexes, and geomorphology back-stripping [30]. We obtained the paleo-water depth using the following steps: Firstly, we studied the types of sedimentary facies developed during each period in the basin, which were then analyzed based on updated data, including cuttings, cores, seismic data, and well logs [16,17,19]. Then, we obtained the paleo-water depth during each period according to the relationship between the water depth and sedimentary facies. Finally, to increase the accuracy, we also compared the results of the relative sea levels in the two basins, which were obtained from previous studies (Figure 2).

But it should be noted that the determination of the facies was based on an integrated analysis of sedimentary and fossil characteristics from various sources, which inevitably has led to mistakes in estimating the paleobathymetry and the subsidence [31]. A number of researchers have conducted studies on eustatic sea-level change [32–34]. In this study, we adopted the results of studies based on borehole data for the continental margin of eastern North America because the tectonic setting and evolution of the northern continental margin of the SCS are very similar to those of the eastern margin of North America [32].

4. Results

4.1. Subsidence Characteristics of Single Wells (1D)

4.1.1. 1D Subsidence Characteristics in the QDNB

In the QDNB, 28 wells were selected to calculate the 1D subsidence (Figure 1), and 12 typical wells were chosen to analyze the spatiotemporal variations in the Cenozoic subsidence of the basin (Figure 3).

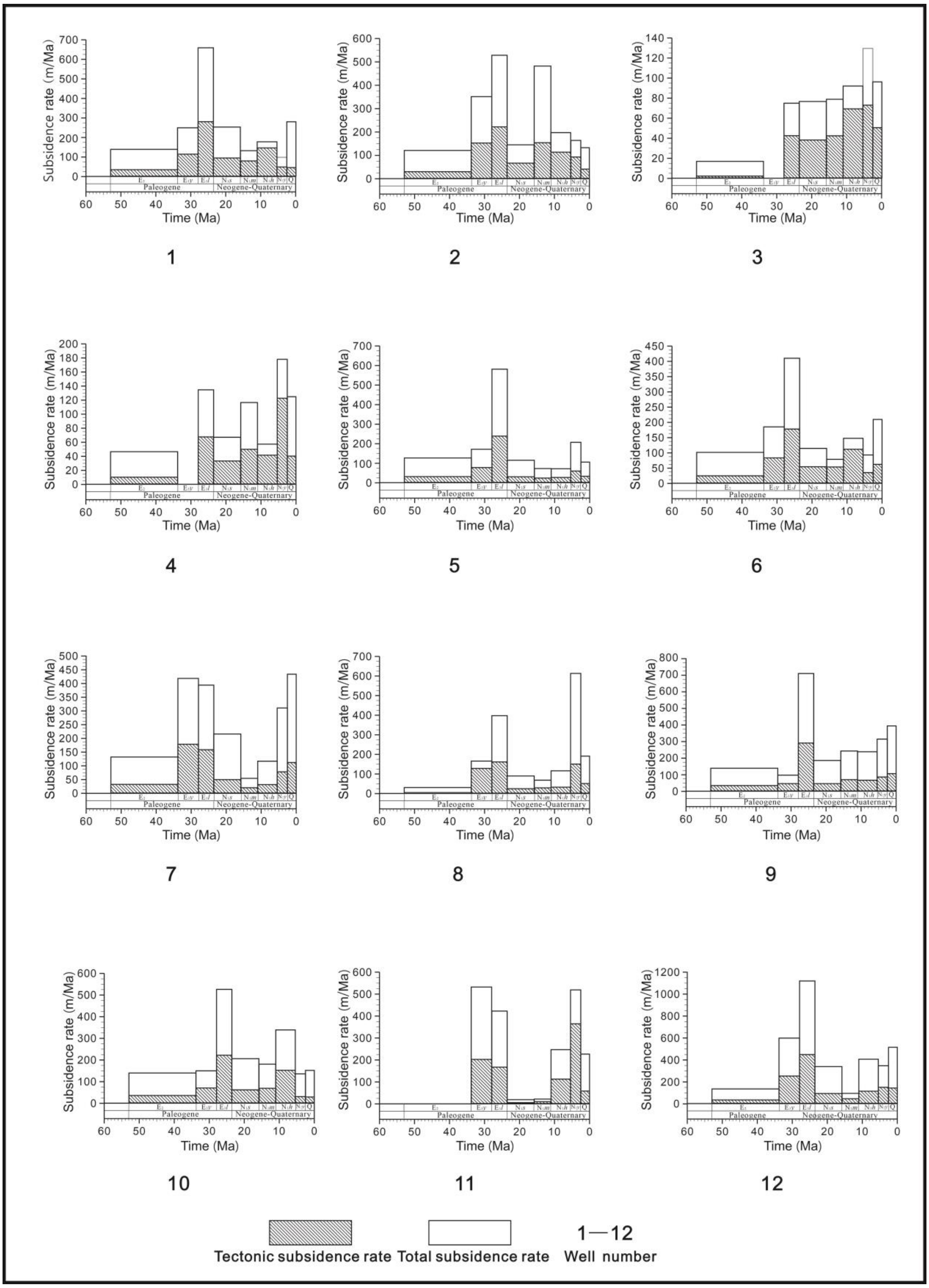

Figure 3. Subsidence rates of typical wells in the QDNB.

In the Eocene, the mean overall subsidence rate (Ra) was 83 m/myr and the mean tectonic subsidence rate (Rt) was 20 m/myr. The mean subsidence rate of one period in this paper was acquired by averaging the subsidence rates of all the wells for that period, which is described in a later section of this paper and was the same situation, so it is not introduced again. Based on the differences between the subsidence rates of the typical wells and the mean subsidence rate, the depocenters were divided into three types: (1) the main depocenters with subsidence rates greater than the mean subsidence rate, (2) the sub-depocenters with subsidence rates close to the mean subsidence rate; and (3) the non-depocenters with subsidence rates lower than the mean subsidence rate. The three types of depocenters are described in a later part of this paper, and the situation was the same, so they are not described here. The Changchang, Songnanbaodao, Songxi, western Ledonglingshui, and northern Huaguang sags were identified as the main depocenters (wells 1, 2, 5, 7, 9, 10, and 12 in Figures 1 and 3). The sub-depocenters were only distributed in the Beijiao sag (wells 3 and 6 in Figures 1 and 3). The Yongle and Yabei sags were the non-depocenters (wells 4 and 8 in Figures 1 and 3). The depocenters with the highest subsidence rates were distributed in the western Ledonglingshui and Yacheng sags. Apart from the Yabei and Yongle sags, the subsidence rates in the other areas were relatively high. Furthermore, the distribution of the main depocenters in the plane was an arc bending toward the north from east to west. In the Early Oligocene, the mean Ra and was 207 m/myr, and the Rt was 89 m/myr. The main depocenters were distributed in the eastern Songnanbaodao, Songxi, Yanan, and western Ledonglingshui sags (wells 2, 7, 11, and 12 in Figures 1 and 3). The Changchang, western Songnanbaodao, and western Beijiao sags were the sub-depocenters (wells 1, 5, and 6 in Figures 1 and 3). The non-depocenters included the eastern Beijiao, Yabei, northwestern Ledonglingshui, Huaguang, and Yongle sags (wells 3, 4, 8, 9, and 10 in Figures 1 and 3). The depocenters with the highest subsidence rates were still distributed in the western Ledonglingshui sag. The total subsidence features were similar to those in the previous period, except for the addition of subsidence areas in the south-eastern and northwestern parts of the basin. In the Late Oligocene, the mean Ra was 391 m/myr, and the mean Rt was 163 m/myr. The Changchang, Songnanbaodao, Ledonglingshui, and Huaguang sags were the main depocenters due to their high subsidence rates (wells 1, 2, 5, 6, 12, and 10 in Figures 1 and 3). The sub-depocenters included the western Beijiao, Songxi, and Yabei sags (wells 6, 7, 8, and 11 in Figures 1 and 3). The non-depocenters included the eastern Yabei and Yongle sags (wells 3 and 4 in Figures 1 and 3). The western Ledonglingshui sag was still the depocenter with the highest subsidence rate. Moreover, the planar distribution of the main depocenters was still a northward arc, and the sub-depocenters were distributed along the two sides of the arc. The southeastern part of the basin became the non-depocenter area, and the northwestern part of the basin became the sub-depocenters, as compared to the previous period. In the Early Miocene, the mean Ra was 129 m/myr, and the Rt was 41 m/myr. The main depocenters were the Changchang, Songxi, Huaguang, and western Ledonglingshui sags (wells 1, 7, 10, and 12 in Figures 1 and 3). The sub-depocenters included the Songnanbaodao sag, the western part of the Beijiao sag, and the northwestern Ledonglingshui and Yanan sags (wells 2, 5, 6, 9, and 11 in Figures 1 and 3). The eastern Beijiao, Yongle, and Yabei sags were the non-depocenters (wells 3, 4, and 8 in Figures 1 and 3). Overall, the subsidence features of this period were the same as those of the previous period, with only slight changes. The western part of the Ledonglingshui sag still had the highest subsidence rate among all units, and the planar distribution of the main depocenters and the sub-depocenters was still an arc bending toward the north, similar to that in the previous periods. However, the northwestern part of the basin became a non-depocenter area. In the Middle Miocene, the average Ra was 93 m/myr, and the mean Rt were and 41 m/myr. The main depocenters were primarily distributed in the Changchang, eastern Songnanbaodao, Yongle, northern Ledonglingshui, and Huaguang sags (wells 1, 2, 4, 9, and 10 in Figures 1 and 3). The only sub-depocenters were the eastern Beijiao and western Ledonglingshui sags (wells 3 and 12 in Figures 1 and 3). The western Songnanbaodao, western Beijiao, Songxi, Yabei, and Yanan sags were the non-depocenters (wells 5, 6, 7, 8, and 11 in Figures 1 and 3). The subsidence features of this period differed from those of the previous period. The depocenters with the largest subsidence rates were now in the northwestern Ledonglingshui sag. The range of the non-depocenters, which were distributed as an NW trending zone, was consistent with the trend of the Yacheng rise and the Lingshui and Songnan low rises and extended toward the inner part of the basin. Nevertheless, the depocenters, including the main and the sub-depocenters, were primarily distributed in the northeastern and southwestern parts of the non-depocenter zones. In the Late Miocene, the mean Ra was145 m/myr, and the mean Rt was 67 m/myr. The main depocenters included the Changchang, eastern Songnanbaodao, Ledonglingshui, and Huaguang sags (wells 1, 2, 9, 10, and 12 in Figures 1 and 3). The only sub-depocenter was the Beijiao sag (wells 3 and 6 in Figures 1 and 3). The Yongle, western Songnanbaodao, Songxi, Yabei, and Yanan sags were the non-depocenters (wells 4, 5, 7, 8, and 11 in Figures 1 and 3). The overall subsidence characteristics were similar to those during the previous period, but once again, the western Ledonglingshui sag became the depocenter with the highest subsidence rate. In addition, the non-depocenter zone, which had the same trend as the Lingshui low rise and the Yacheng and Songtao rises, shifted northward. In the Pliocene, the average Ra was 227 m/myr, and the average Rt was 79 m/myr. The Songxi, Yabei, Ledonglingshui, and Yanan sags were the main depocenters (wells 7, 8, 9, 12, and 11 in Figures 1 and 3). However, the sub-depocenters were primarily distributed in the Songnanbaodao, Yongle, and eastern Beijiao sags (wells 2, 5, 3, and 4 in Figures 1 and 3). The non-depocenter areas included the Changchang, western Beijiao, and Huaguang sags (wells 1, 6, and 10 in Figures 1 and 3). The subsidence features during this period were completely different from those of the previous periods. The depocenter with the largest subsidence rate was the Yabei sag, and the scope of the non-depocenters expanded toward the north, with a NE trend that was consistent with the trend of the Lingnan low rise and the Beijiao rise. The depocenters, including the main and the sub-depocenters, were distributed along the two sides of the non-depocenter zone, and the subsidence rate increased with increasing distance from the non-depocenter zone. In the Quaternary, the mean Ra was158 m/myr, and the mean Rt was 108 m/myr. The subsidence characteristics changed dramatically because the controlling factors varied from one area to another, and an anomalous subsidence occurred during this period. The northern part of the basin, e.g., the western Songnanbaodao, Songxi, Yabei, western Ledonglingshui, and Yanan sags (wells 5, 7, 8, 9, 11, and 12 in Figures 1 and 3), was characterized by a high Ra and a low Rt. In contrast, the southern part of the basin, e.g., the Changchang, eastern Songnanbaodao, Beijiao, Yongle, and Huaguang sags (wells 1, 2, 3, 4, 6, and 10 in Figures 1 and 3), was characterized by a low Ra and a high Rt.

The above analysis of the subsidence evolution indicated that from the Eocene to the Early Miocene, the subsidence features had remained similar overall. The northwestern and southeastern parts of the basin, especially the eastern Beijiao and Yongle sags, were the non-depocenter areas. The other areas of the basin were the depocenters, which were distributed in an arc shape, bending toward the north on a plane from east to west. The subsidence characteristics in the Middle and Late Oligocene were completely different from those during the previous periods, and the subsidence was characterized by the extension of the non-depocenter areas. The distribution of the non-depocenter areas during the Middle Miocene remained consistent with the trend of the Yacheng rise, Lingshui low rise, Songtao rise, and Songnan low rise, but it shifted to follow the trend of the Yacheng rise, Lingshui low rise, and Songtao rise in the Late Miocene. Generally, the depocenter areas were primarily distributed in the northeastern and southwestern parts of the basin, which had been separated by the non-depocenters during the Middle and Late Miocene periods. The subsidence features completely changed during the Pliocene. Most of the southern parts of the basin became the non-depocenters, the trend of which was consistently distributed with the Lingnan low rise and Beijiao rise, due to the northward migration of the depocenter areas. In the Quaternary, an anomalous subsidence occurred in the southern part of the basin.

4.1.2. 1D Subsidence Characteristics in the YGHB

In the YGHB, 16 wells were selected to calculate the 1D subsidence history, from which 12 typical wells were chosen to analyze the spatiotemporal variations in the subsidence of the basin (Figure 4). Because of the lack of exploration, only limited seismic and well data, along with limited information about the thick strata in the YGHB, were available. The strata systems of the basin that have been comprehensively studied include the Upper Oligocene and the Quaternary strata. Correspondingly, the time span of the subsidence history of the YGHB investigated in this paper was from the Late Oligocene to the Quaternary.

In the Late Oligocene, the mean Ra and Rt were 603 m/myr and 212 m/myr, respectively. The subsidence area was limited, and the main depocenters were distributed in the northwestern Yinggehai sag and the southeastern Linggao rise (wells 10, 11, and 12 in Figures 1 and 4). The non-depocenter areas were distributed only in the contact area between the northwestern Yinggehai sag and the southeastern Linggao rise (well 9 in Figures 1 and 4). In the Early Miocene, the average Ra was 159 m/myr, and the average Rt was 48 m/myr. The scope of the depocenter areas had extended further south during this period. The middle part of the Yinggehai sag was the main depocenter (wells 6 and 7 in Figures 1 and 4). The sub-depocenters were primarily distributed in the northeastern Yinggehai sag, which was located next to the Yingdong slope (wells 5, 9, and 10 in Figures 1 and 4). However, the northwestern Yinggehai sag and southeastern Linggao rise became the non-depocenters during this period (wells 11 and 12 in Figures 1 and 4). In the Middle Miocene, the mean Ra was 446 m/myr, and the mean Rt was 129 m/myr. The range of the depocenters persistently expanded southerly, as compared to their range during the previous period, and the entirety of the Yingdong slope subsided synchronously with different subsidence rates, which varied by location. The main depocenters were distributed in the southeastern Yinggehai sag and the Yingdong slope (wells 1, 2, and 3 in Figures 1 and 4). The main depocenters during the previous period became the sub-depocenters during this period (wells 6 and 7 in Figures 1 and 4). The northwestern part of the basin became the non-depocenter area (wells 5, 8, 9, 10, 11, and 12 in Figures 1 and 4). In the Late Miocene, the mean Ra and Rt were 87 m/myr and 21 m/myr, respectively. The subsidence features of this period were completely different from those of the previous periods, and the depocenters migrated to the northwestern part of the basin. The main depocenters were primarily distributed in the central and northwestern parts of the Yinggehai sag, the northwestern Yingdong slope, and the southeastern Linggao rise (wells 3, 6, 8, 10, 11, and 12 in Figures 1 and 4). The sub-depocenters were distributed in the western Yingge sag and the southeastern Linggao rise (wells 7 and 9 in Figures 1 and 4). The central and southeastern parts of the Yingdong slope, as well as the adjacent area, became the non-depocenter areas during this period (wells 1, 2, 4, and 5 Figures 1 and 4). In the Pliocene, the mean Ra was 483 m/myr, and the mean Rt was 130 m/myr. The main depocenters were concentrated in the central Yinggehai sag (wells 2, 3, 5, 6, and 7 in Figures 1 and 4). However, the contact area between the Yinggehai sag and the Linggao rise became the sub-depocenter area (wells 9, 10, and 11 in Figures 1 and 4). In addition, the entire Yingdong slope and the northwestern Yinggehai sag became the non-depocenter areas (wells 1, 4, 8, and 12 in Figures 1 and 4). The subsidence characteristics changed, as compared to the previous period. For example, the depocenters shifted from the northwest to the central part of the basin, and most of the non-depocenters were distributed on the Yingdong slope. In the Quaternary, the mean Ra was 140 m/myr, and the Rt was 27 m/myr. The overall subsidence features only changed slightly and were similar to those of the previous period overall. The range of the depocenters shrank, and they were distributed in the southeastern part of the basin, which caused the northwestern part of the basin to become the non-depocenter area. The main depocenters were distributed in the southeastern Yinggehai sag (wells 2 and 3 in Figures 1 and 4). However, the central Yinggehai sag and the northwestern Yingdong slope became the sub-depocenters (wells 5, 6, 7, and 8 in Figures 1 and 4). The non-depocenters were primarily distributed in the northeastern and northwestern parts of the basin (wells 1, 4, 9, 10, 11, and 12 in Figures 1 and 4).

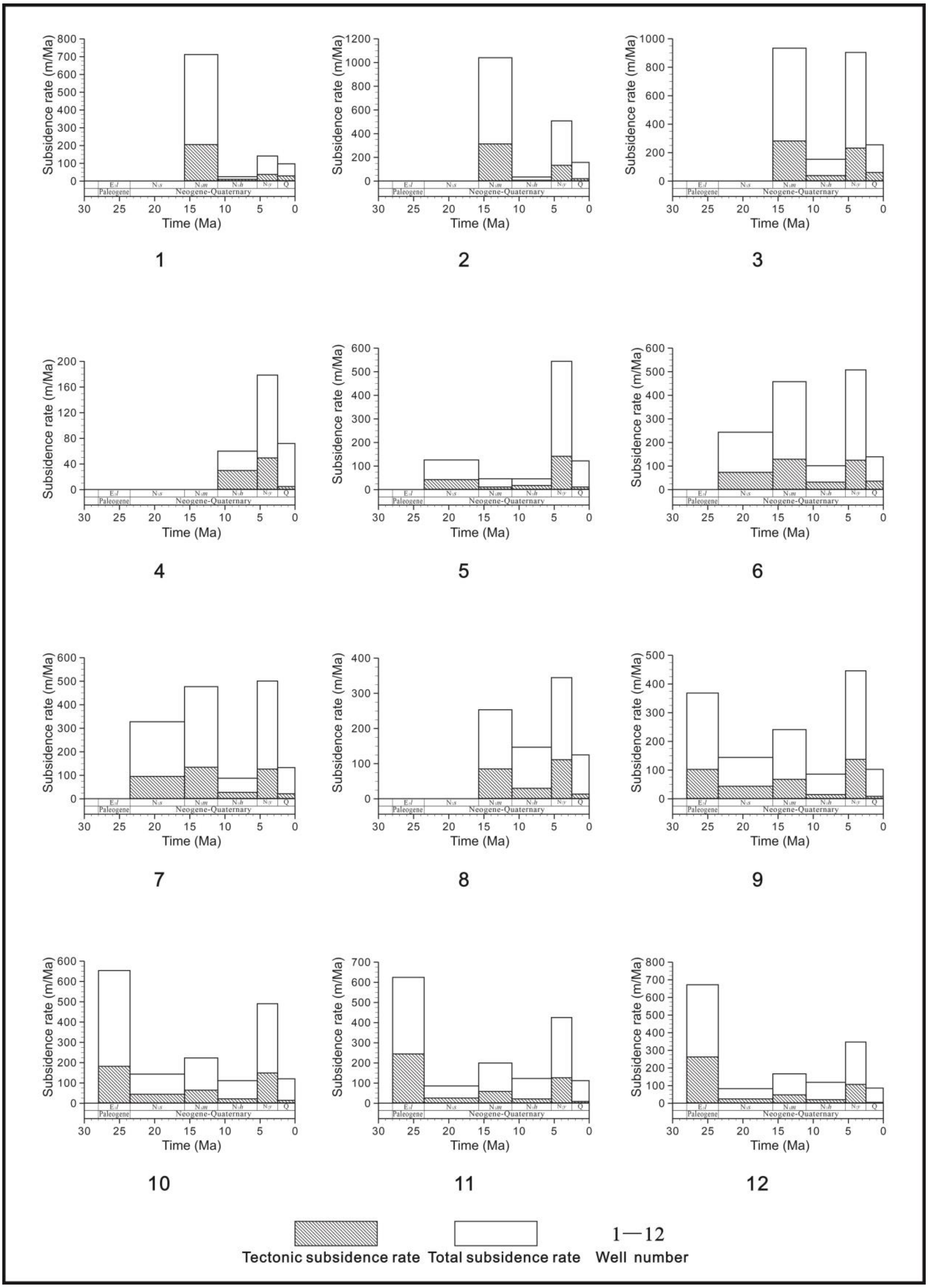

Figure 4. Subsidence rates of typical wells in the YGHB.

Based on the above analysis, we found that the spatiotemporal variations in the subsidence had changed regularly. From the Late Oligocene to the Middle Miocene, the depocenters had continuously shifted southeast, and the range of the depocenter area had expanded progressively. In the Late Miocene, the depocenters had migrated toward the northwest, and the range of the depocenter area was the largest, although the subsidence rate was relatively small. From the Pliocene to the present, the depocenters shifted to the east, and the scope of the depocenter area decreased. Consequently, the northwestern part of the basin became the non-depocenter area. The Late Miocene was an obvious and critical turning point, before and after which the subsidence features were dramatically different.

4.2. Subsidence Characteristics of Profiles (2D)

4.2.1. 2D Subsidence Characteristics in the QDNB

Six seismic profiles of the QDNB were studied, among which one profile in the eastern basin was selected to analyze the spatiotemporal variations in the 2D subsidence characteristics.

In the eastern part of the basin, the subsidence area was limited, and it only included the Songnanbaodao sag and the Baodao rise in the Eocene (Figure 5). The depocenters were primarily distributed in the Songnanbaodao sag, which experienced the maximum subsidence, reaching approximately 2420 m by the end of the Eocene. In the Early Oligocene, the scope of the subsidence, including several main depocenters, expanded to some extent, as compared to the previous period. By the end of the Early Oligocene, the maximum subsidence of the Yacheng Formation had reached 2900 m. In the Late Oligocene, the scope of the subsidence, which was characterized by nearly unchanged subsidence features, increased further. Moreover, the main depocenters were still distributed in the Songnanbaodao sag, and the maximum subsidence of the Lingshui Formation increased to 3080 m at the end of the Late Oligocene. In the Early Miocene, the subsidence features changed slightly, but the Songnanbaodao sag was still the area in which the maximum subsidence of the Sanya Formation had occurred, reaching approximately 1780 m by the end of the Early Miocene. For example, the stratum was distributed as a blanket in the plane, which led to a decrease in the subsidence differences between the depocenters. In addition, the subsidence in the Beijiao sag and the Beijiao rise decreased because these two tectonic units were uplifted during this period. During the Middle Miocene, the subsidence features varied significantly, except in the Songnanbaodao and Yongle sags. The subsidence of the northern Baodao rise, Beijiao sag, and Beijiao rise were small due to the remarkable amount of uplift. At the end of the Middle Miocene, the largest subsidence of the Meisha Formation was 1020 m. While in the Late Miocene, the subsidence characteristics of the Songnanbaodao sag, where the greatest subsidence of the Huangliu Formation reached 1050 m by the end of the Late Miocene, remained nearly unchanged. However, the subsidence features of the remaining areas changed dynamically. For example, the subsidence in the Beijiao sag was relatively large because it had subsided sharply during this period. The non-depocenters were distributed in the Beijiao rise and Yongle sag due to an incessant uplift. The subsidence features of all the areas changed in the Pliocene, during which the depocenters moved to the two sides of the locations of the depocenters during the previous period. The largest subsidence of the Yinggehai Formation increased to 1800 m by the end of the Pliocene and was located in the river channel. The uplift of the Beijiao had continued during this period, while the Yongle sag had subsided slightly. From the Quaternary to the present, the seawater intruded into the eastern QDNB with a large water depth because a transgression had begun during this period [14].

Based on the above analysis, we found that the differences in the subsidence of each unit were relatively high from the Eocene to the Oligocene. The reason for this was that this period was the rifting stage when the faults primarily developed, which had resulted in the development of the various grabens and half-grabens where the subsidence had occurred. However, after the Miocene, the differences in the subsidence of the tectonic units decreased. In the Pliocene, the southern part of the basin had been uplifted, and the northern part of the basin had subsided.

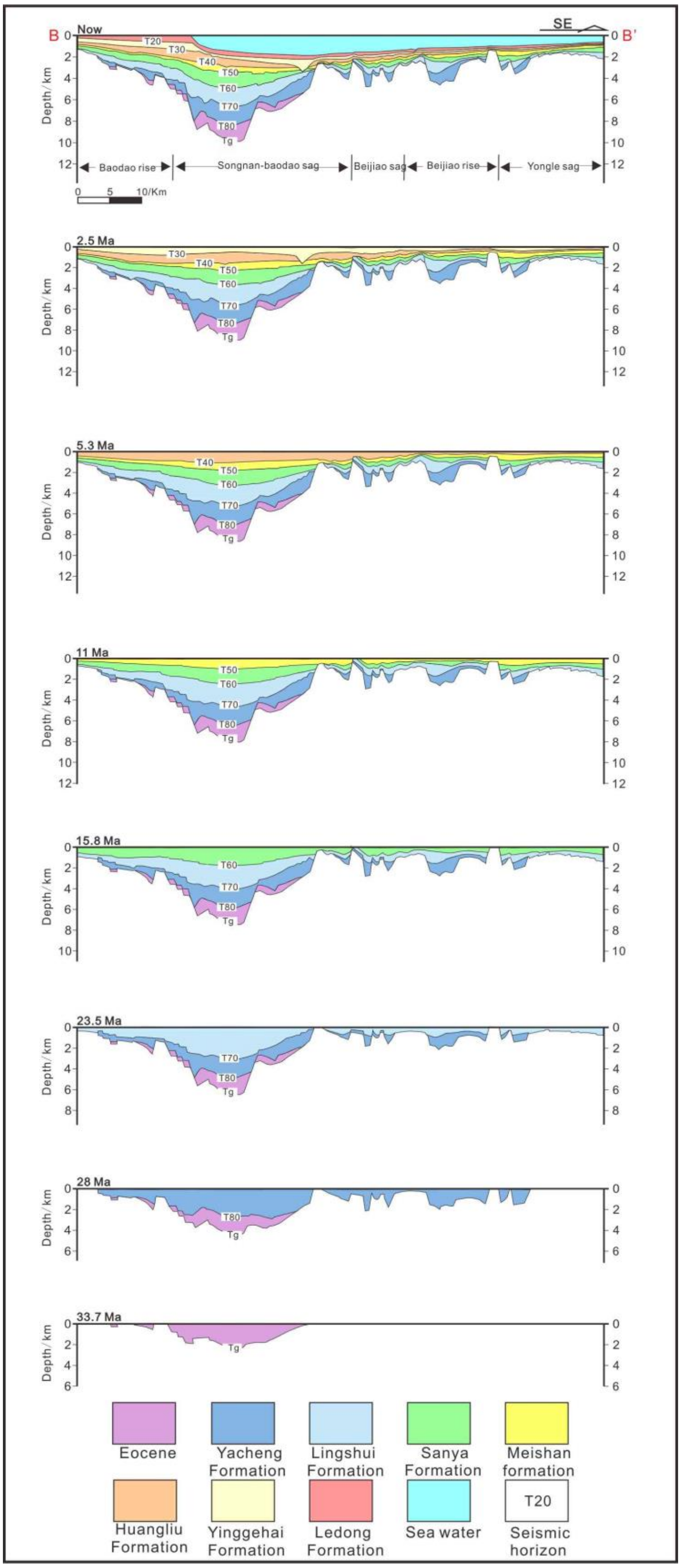

Figure 5. Regional subsidence evolution profiles in the QDNB (original profile from ref. [19], For location of the profile, see Figure 1).

4.2.2. 2D Subsidence Characteristics in the YGHB

In the YGHB, three seismic profiles distributed in the southern, central, and northern parts of the basin were analyzed, among which we selected the central profile to analyze the spatiotemporal variations of the subsidence in the basin. The YGHB was characterized by a low exploration level and a thick stratum in the central basin. In addition, due to the low quality of the seismic data, the stratum that could be used to analyze the subsidence history only included the Sanya Formation and the overlying formations (Figure 6).

In the Early Miocene, subsidence only occurred in the Yinggehai sag. The largest subsidence of the Sanya Formation was 2380 m by the end of the Early Miocene. In the Middle Miocene, the subsidence had still only occurred in the Yinggehai sag, but the amount of subsidence was significant, particularly in the central part of the sag. The shape of the profile of the Meishan Formation was a wedge because its thickness had increased gradually from east to west. The maximal subsidence of the Meishan Formation reached 3150 m at the end of the Middle Miocene. The subsidence characteristics had changed distinctly in the Late Miocene. For example, the subsidence range had expanded to the Yingdong slope. In addition, the thickness of the stratum varied significantly in the horizontal direction; however, the Yinggehai sag was still the area where the maximal subsidence of the Huangliu Formation occurred, reaching only 910 m by the end of the Late Miocene. Until the Pliocene, the subsidence features had only changed slightly. The scope of the subsidence remained unchanged, but the amount of subsidence varied significantly from the Yinggehai sag to the Yingdong slope because the former unit had experienced a large amount of subsidence and was the area where the depocenters had been distributed. In contrast, the latter unit was the area where the non-depocenters had been distributed due to its relatively small amount of subsidence. At the end of the Pliocene, the largest subsidence of the Yinggehai Formation was 2430 m. Since the Quaternary, the subsidence has increased gradually from west to east, but the largest subsidence of the Ledong Formation was still located in the Yinggehai sag, reaching 1090 m by the end of the Quaternary.

Based on the above analysis, we found that the subsidence of the YGHB during the Cenozoic was as follows. First, the Yinggehai sag, which had continuously subsided since the Miocene, was the main area where the depocenters had been distributed. However, the Yingdong slope had been uplifted on a large scale from the Early Miocene to the Middle Miocene, and on a small scale, during the Late Miocene, which had resulted in a lack of subsidence during the former two periods. Second, the YGHB was characterized by episodic subsidence during the Cenozoic based on the 2D subsidence characteristics, that is, the subsidence had changed in an orderly manner over time. For example, the subsidence had been significant in the Middle Miocene and Pliocene but minor during the Early Miocene, Late Miocene, and Quaternary.

4.3. Holistic Subsidence of the Entire Basin

To reveal the holistic subsidence of the entire basin, based on the subsidence differences between the two basins and the controlling factors of this phenomenon, we weighted all the well data to determine the holistic subsidence (Figures 7 and 8).

4.3.1. Holistic Subsidence of the QDNB

The holistic subsidence of the QDNB was episodic. According to the changes in the subsidence process, the holistic subsidence process of the QDNB consisted of three episodes. The first one occurred during the Eocene; the second episode occurred during the Oligocene and Middle Miocene; and the third episode occurred from the Late Miocene to the Quaternary (Figure 7).

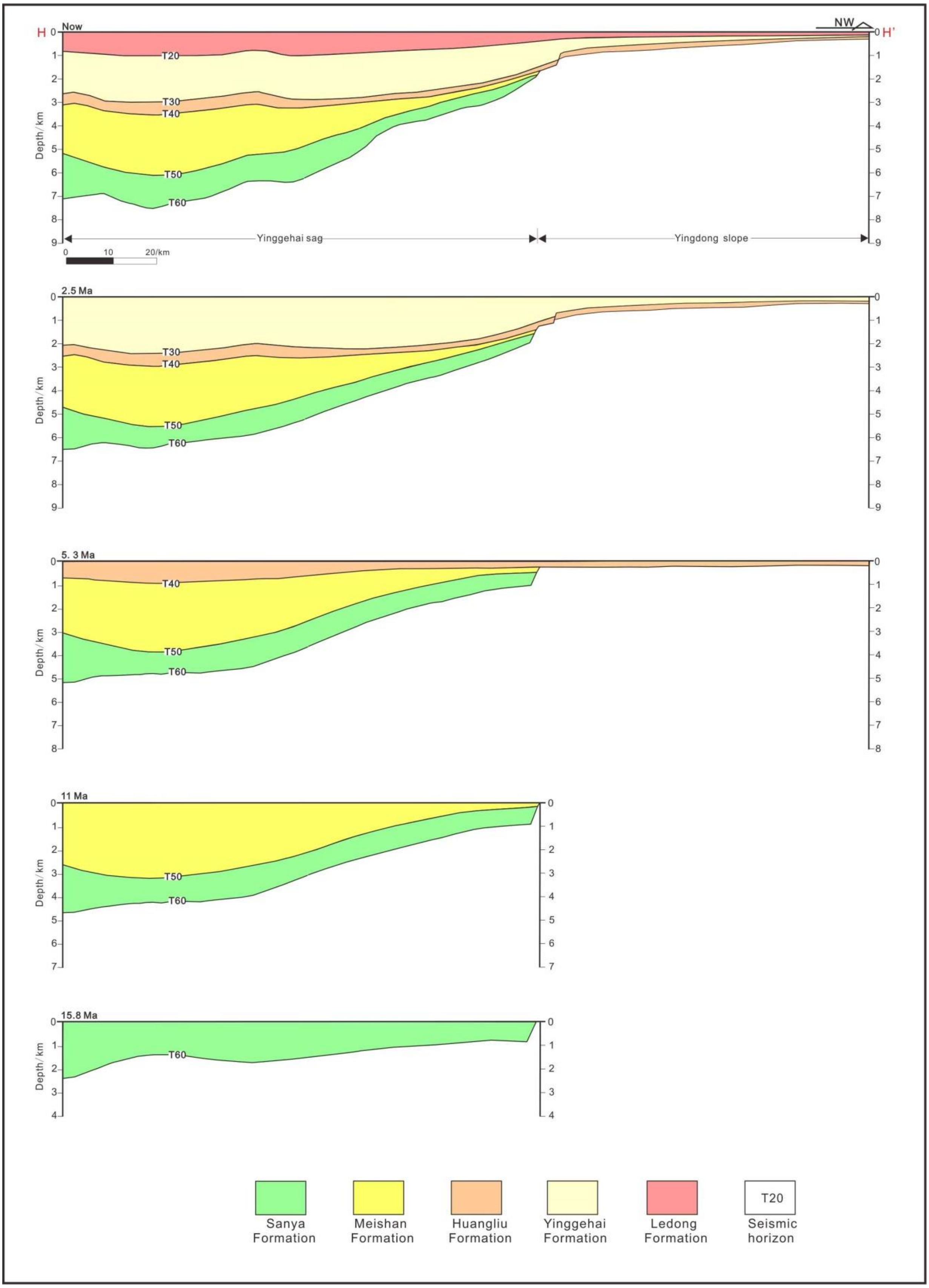

Figure 6. Regional subsidence evolution profile in the western YGHB (original profile from ref. [19]; for location of the profile, see Figure 1).

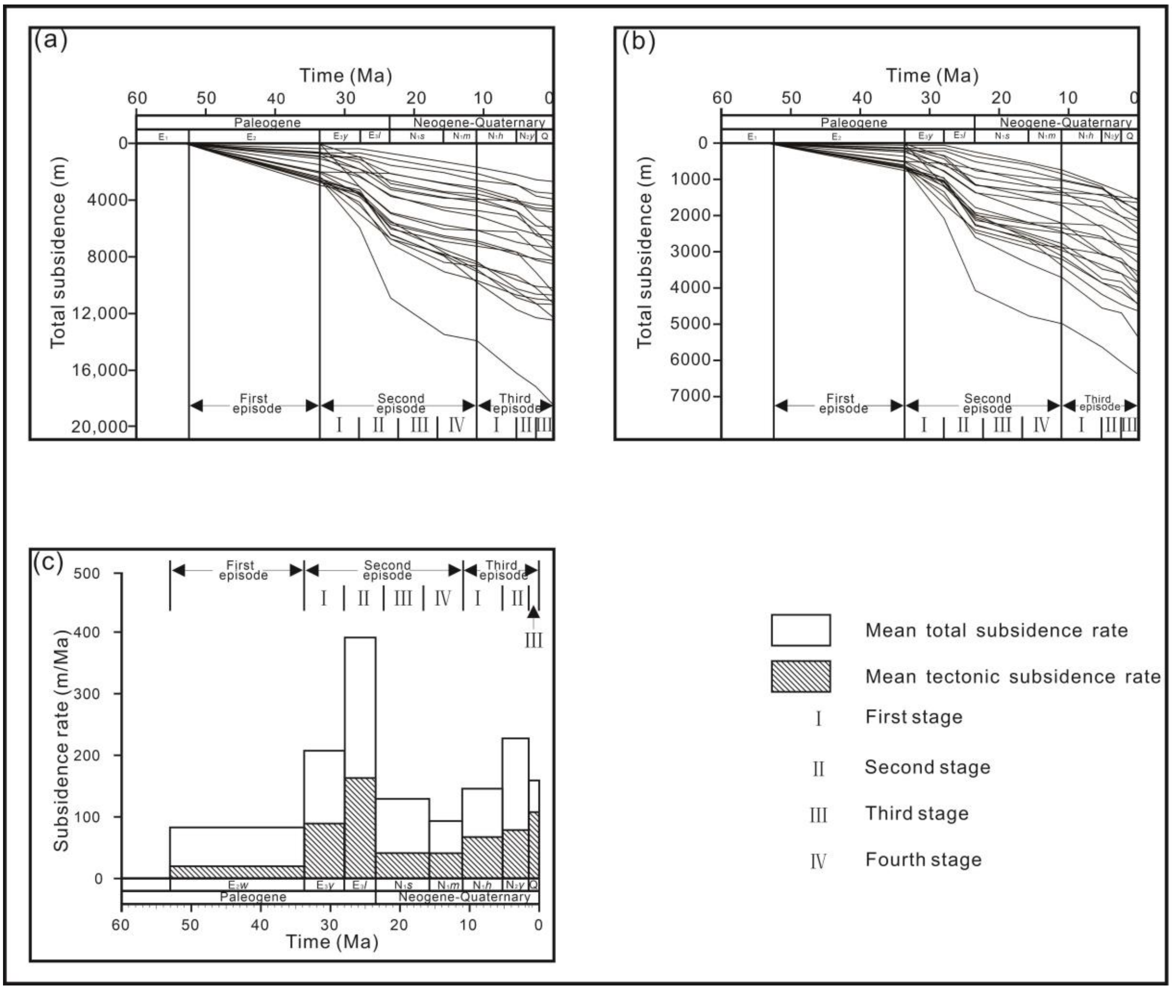

Figure 7. Holistic subsidence curves and subsidence rates in the QDNB: (**a**) total subsidence curve; (**b**) tectonic subsidence rate; (**c**) holistic total subsidence rate and holistic tectonic subsidence rate, which were acquired by averaging 28 wells. The lines in (**a**,**b**) are the subsidence curves of 28 fictitious wells.

During the first episode, the mean Ra was 80 m/myr, and the mean Rt was 20 m/myr, which only comprised 25% of the overall subsidence. During the second episode, because the subsidence rate increased, the Ra increased to 205 m/myr, and the Rt grown to 83.5 m/myr. In this study, the mean subsidence rate of a single episode was acquired by averaging the mean subsidence rates of all the periods in that episode (Figure 7). This is described in the latter part of the paper for the same situation and, thus, is not provided here. The proportion of the tectonic subsidence that occurred during the second episode comprised 40.7% of the Ra. Moreover, according to the changes in the subsidence rate, the second episode was divided into four stages. The first stage occurred in the Early Oligocene, during which the mean Ra was 207 m/myr, and the mean Rt was 89 m/myr. The tectonic subsidence during this stage comprised 42.9% of the overall subsidence. The second stage occurred in the Late Oligocene, during which the subsidence rate reached the maximum during the entire evolution of the basin. The mean Ra was 391 m/myr, the mean Rt was 163 m/myr, and the tectonic subsidence comprised 41.7% of the overall subsidence. The third stage occurred in the Early Miocene, during which the mean Ra and Rt were 129 m/myr and 41 m/myr, respectively. The tectonic subsidence during this stage comprised 31.8% of the overall subsidence. The fourth stage occurred in the Middle Miocene, during which the mean Ra was 93 m/myr and the mean Rt was still 41 m/myr (i.e., unchanged, as compared to the previous stage), accounting for 44.1% of the Ra. In the third episode, the mean Ra was 177 m/myr, and the mean Rt was 84 m/myr, comprising

47.5% of the Ra. Similar to the situation during the previous episode, the third episode was also divided into three stages. The first occurred during the Late Miocene. The mean Ra was 145 m/myr, and the mean Rt was 67 m/myr, so the tectonic subsidence comprised 46.2% of the overall subsidence. The second stage occurred during the Pliocene. The mean Ra was 227 m/myr, which was the highest rate during the entire third episode, and the mean Rt was 79 m/myr, accounting for 34.8% of the Ra. The third stage occurred during the Quaternary. The mean Ra was 159 m/myr, and the mean Rt was 108 m/myr. The tectonic subsidence comprised 67.9% of the overall subsidence and reached the highest rate during the entire evolution of the basin.

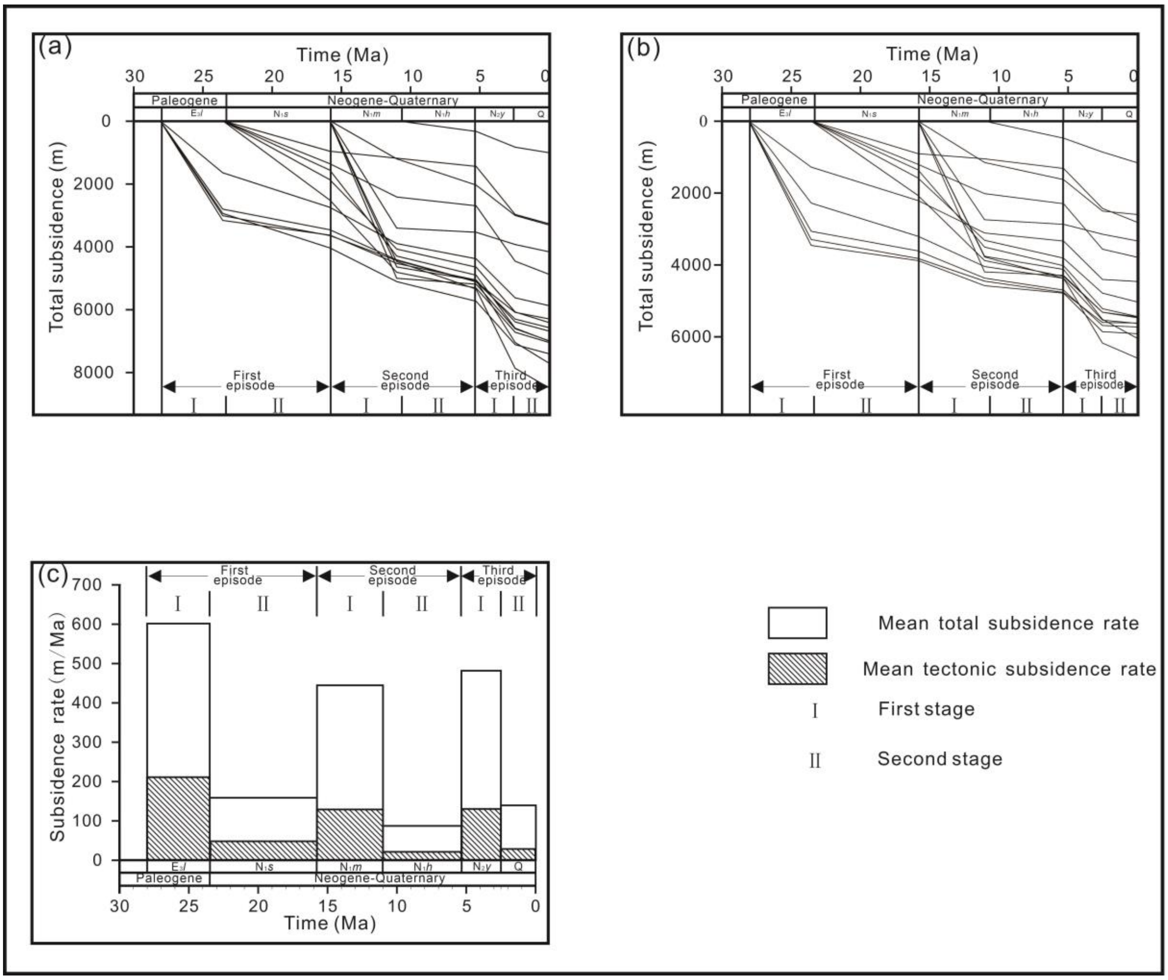

Figure 8. Holistic subsidence curves and subsidence rates in the YGHB: (**a**) total subsidence curve; (**b**) tectonic subsidence rate; (**c**) holistic total subsidence rate and holistic tectonic subsidence rate, which were acquired by averaging 16 wells. The lines in (**a**,**b**) are the subsidence curves of 16 fictitious wells.

Based on the above analysis, we concluded that the subsidence rate was low during the first episode, peaked during the second episode, and decreased in the third episode. However, the percentage of the overall subsidence determined by the tectonic subsidence increased continuously during the entire evolution of the basin, and it reached the high rate during the Quaternary.

4.3.2. Holistic Subsidence of the YGHB

The holistic subsidence of the YGHB was characterized by more distinct episodes, as compared to the QDNB. Based on the changes in the subsidence rate, since the Late Oligocene to the Quaternary, the basin subsidence process was divided into three episodes.

The first episode occurred from the Late Oligocene to the Early Miocene; the second episode occurred from the Middle Miocene to the Late Miocene; and the third episode occurred from the Pliocene to the Quaternary (Figure 8).

During the first episode, the mean Ra was 381 m/myr, the mean Rt was 130 m/myr, and the tectonic subsidence comprised 34.1% of the overall subsidence. This episode was further divided into two stages. The first stage occurred during the Oligocene, and the maximal subsidence rate in the entire basin subsidence process occurred during this period. During this stage, the mean Ra was 603 m/myr, and the mean Rt was 212 m/myr, comprising 35.1% of the Ra. The second stage, which was characterized by a sharp decrease in the subsidence rate, occurred in the Early Miocene. The mean Ra was 159 m/myr, and the mean Rt was 48 m/myr, accounting for 30.2% of the Ra. During the second episode, the subsidence rate lessened to some extent, and the mean Ra was 266.5 m/myr, and the mean Rt was 75 m/myr. The tectonic subsidence comprised 28.1% of the overall subsidence. Similarly, the second episode was separated into two stages. The first stage occurred during the Middle Miocene. The subsidence rate increased, the mean overall subsidence increased to 446 m/myr, and the mean Rt increased to 129 m/myr, accounting for 28.9% of the Ra. The second stage occurred during the Late Miocene. The minimum subsidence rate in the entire evolution of the basin occurred during this stage. The mean Ra was 87 m/myr, and the mean Rt was 21 m/myr. The tectonic subsidence comprised 24.1% of the overall subsidence. The third episode occurred in the Pliocene and Quaternary. The mean Ra was 311.5 m/myr, and the mean Rt was 78.5 m/myr, comprising 25.2% of the Ra. The third episode consisted of two stages. The first stage occurred in the Pliocene, during which the subsidence rate increased. The mean Ra was 483 m/myr, and the mean Rt was 130 m/myr, comprising 26.9% of the overall subsidence. The second stage occurred in the Quaternary, during which the subsidence rate was low. The mean Ra was 140 m/myr, and the mean Rt was only 27 m/myr, comprising 19.2% of the Ra.

The above analysis indicated that the most significant subsidence feature of the YGHB was the dramatically different episodes. Each subsidence episode consisted of a stage with a high subsidence rate and a stage with a low subsidence rate. In addition, the subsidence rate was high during the first episode and then decreased during the second and third episodes.

5. Discussion

5.1. Relationship between the Basin Subsidence and Tectonics

The QDNB and the YGHB were surrounded by the Indian, Eurasian, and Pacific plates in the Cenozoic. The interactions among these three plates have induced several particular geological processes, including the uplift of the Tibetan Plateau, the strike-slip motion of the Red River Fault, and the expansion of the SCS, all of which have influenced the basin evolution and subsidence. However, the effects of these three geological processes on the basin have varied for each basin due to the differences in their tectonic locations.

In the QDNB, the subsidence rate was low during the Eocene (Figure 9), and the northwestern and southeastern parts of the basin were the non-depocenters, according to our previous analysis (wells 4 and 8 in Figures 1 and 3). This was because, during the Eocene, the Indian Plate had moved northeastward [35], and the Pacific Plate had subducted under the Eurasian Plate [36]. Moreover, the rate of the movement of the Indian Plate toward the Eurasian Plate had been higher than the subduction rate of the Pacific Plate, relative to the Eurasian Plate, so there had been enough space to accommodate the mantle material under the South China Block, which had flowed from the northwest to the southeast [37]. Consequently, NE trending grabens and half-grabens developed under the comprehensive influence of these factors. The subsidence only occurred in these grabens and half-grabens. Therefore, the mean total subsidence of the entire basin was low. During the Early Oligocene, the influence of the flow of the mantle material had increased further, and the scale of the rifting increased significantly. Moreover, the SCS had also opened at 32 Ma [38], so the subsidence rate and the scale of the QDNB increased during this period.

The spreading rate of the SCS increased from the late Early Oligocene onwards, and then it peaked at the end of the Late Oligocene, which also caused the subsidence rate of the QDNB to reach its maximum during the Late Oligocene. The subsidence rate was also the highest during the entire evolution of the basin. The spreading of the SCS began to weaken in the Miocene, and it ceased at the end of the Early Miocene, which led to a rapid decrease in the subsidence rate and subsidence scale during the entire Miocene. In the Pliocene, a large-scale regional thermal event had occurred in the QDNB and the YGHB [39], and the dextral strike-slip motion of the Red River Fault had also commenced in the Pliocene. Thus, the subsidence rate of the QDNB increased again under the combined effects of these two geological processes. In the Quaternary, the subsidence rate of the QDNB decreased due to the smaller amount of dextral strike-slip of the Red River Fault. Similar to the other basins all over the world [40], one of the most obvious subsidence features of the QDNB was the anomalous tectonic subsidence that occurred in the Quaternary (wells 1, 2, 3, 4, 6, and 10 in Figures 1 and 3). These sags were characterized by a low total subsidence rate and a high tectonic subsidence rate in the Quaternary. Regarding the cause of this phenomenon, several researchers proposed the thermal cooling after the late magmatism [5]; however, other researchers have proposed a lower crustal flow as an explanation [41]. Based on the previous analysis, we found that the variations in the subsidence over time in the QDNB matched the changes in the flow of the mantle material in the Eocene and the variations in the spreading of the SCS from the Oligocene to the Miocene. However, since the Pliocene, the subsidence features have primarily been controlled by the comprehensive influence of the strike-slip motion of the Red River Fault and the thermal event.

In the YGHB, the subsidence rate had been high in the Late Oligocene (Figure 9), and the subsidence had primarily occurred in the western part of the basin (Figures 1 and 3). During this period, the uplift of the Tibetan Plateau ceased [42], which provided a sufficient sediment source. Accordingly, the scale of the strike-slip movement of the Red River Fault was significant during this period and provided large spatial accommodation because it had consumed the energy of the Indian Plate as it moved northeastward. Consequently, the subsidence rate reached its peak during the entire evolution. During the Early Miocene, the Tibetan Plateau began its second stage of uplift. In addition, in the Miocene, the strike-slip movement of the Red River Fault gradually became weaker because the Indian Plate had started to wedge into the Eurasian Plate [43], which resulted in the southeastward movement of the Eurasian Plate [44], but the velocity of the Eurasian Plate was slower than that of the Indochina Block. Thus, the subsidence rate had decreased in the Early Miocene. During the early Middle Miocene, the Tibetan Plateau remained static, but there was a certain amount of strike-trip movement of the Red River Fault that resulted in the subsidence rate being higher than during the previous period but lower than in the Late Oligocene. During the Late Miocene, the strike-slip movement of the Red River Fault nearly ceased, so the subsidence rate decreased even though the uplift of the Tibetan Plateau had stopped in the Late Miocene. In the Pliocene, the subsidence rate of the YGHB increased again and was higher than during the previous period. This was also the result of the comprehensive influence of the fast dextral strike-slip of the Red River Fault and the thermal event. In the Quaternary, the strength of the dextral strike-slip of the Red River Fault weakened, so the subsidence rate decreased. According to the previous analysis, we found that the subsidence characteristics of the YGHB were primarily controlled by the uplift of the Tibetan Plateau and the strike-slip motion of the Red River Fault before the Middle Miocene; however, the spreading of the SCS may have also contributed to the subsidence characteristics from the Late Oligocene to the Early Miocene. Since the Middle Miocene, the subsidence characteristics have primarily been controlled by the strike-slip movement of the Red River Fault, rather than by the uplift of the Tibetan Plateau. This was because during the first two stages of the uplift of the Tibetan Plateau, the strike-slip motion of the Red River Fault and the uplift of the Tibetan Plateau had been the two main consumers of the energy of the northeastward motion of the Indian Plate [42]. Therefore, the uplift of the Tibetan Plateau had been coupled with the strike-slip motion of the Red

River Fault [43,45], which then had controlled the subsidence characteristics of the YGHB. In the Middle Miocene, the Indian Plate had started to wedge into the Eurasian Plate [44], the Tibetan Plateau had uplifted through the large scale of the over-thrust tectonism, delamination, and melting of the lithosphere [42], which could not be coupled with the strike-slip movement of the Red River Fault and, thus, dramatically affected the subsidence characteristics of the YGHB.

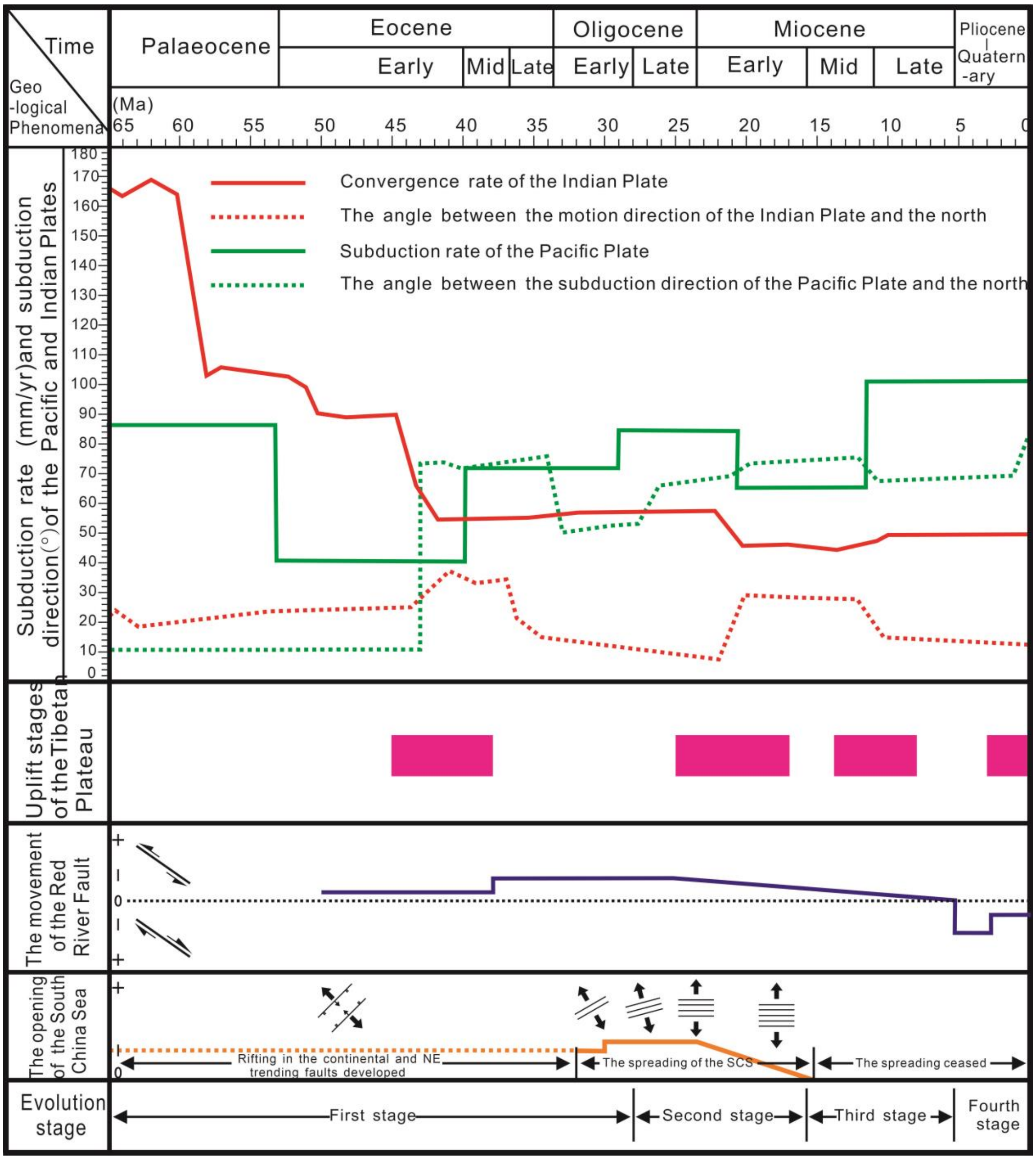

Figure 9. The evolutions of the geological phenomena surrounding the QDNB and the YGHB (i.e., the uplift stage of the Tibetan Plateau, according to Zhong et al. [42]). The movement of the Red River Fault was modified based on Sun et al. [43]. The spreading of the South China Sea was according to Yao [37] and Briais et al. [38].

5.2. Effect of the Faults on the Basin Subsidence

Major faults are always the boundaries of basins and tectonic units, and they determine the structural framework of a basin and play an important role in a basin's evolution, sedimentation, filling, and gas migration and release [46]. Abundant faults have developed in the SCS and its surrounding areas, which have been classified as lithospheric faults, crustal faults, and basement faults, according to their depths [47]. The QDNB and the YGHB are separated by a lithospheric fault (Figure 10). In the QDNB, there are three groups of faults: NW trending, NE trending, and nearly WE trending. The nearly WE trending faults distributed in the eastern part of the basin and the NW trending faults distributed in the western part of the basin are lithospheric faults. The NW trending and NE trending faults are distributed in the interior of the basin and are crustal and basement faults. Three NW trending faults have developed in the YGHB. The fault in the northeastern part of the basin is a lithospheric fault, and the other two faults are basement faults.

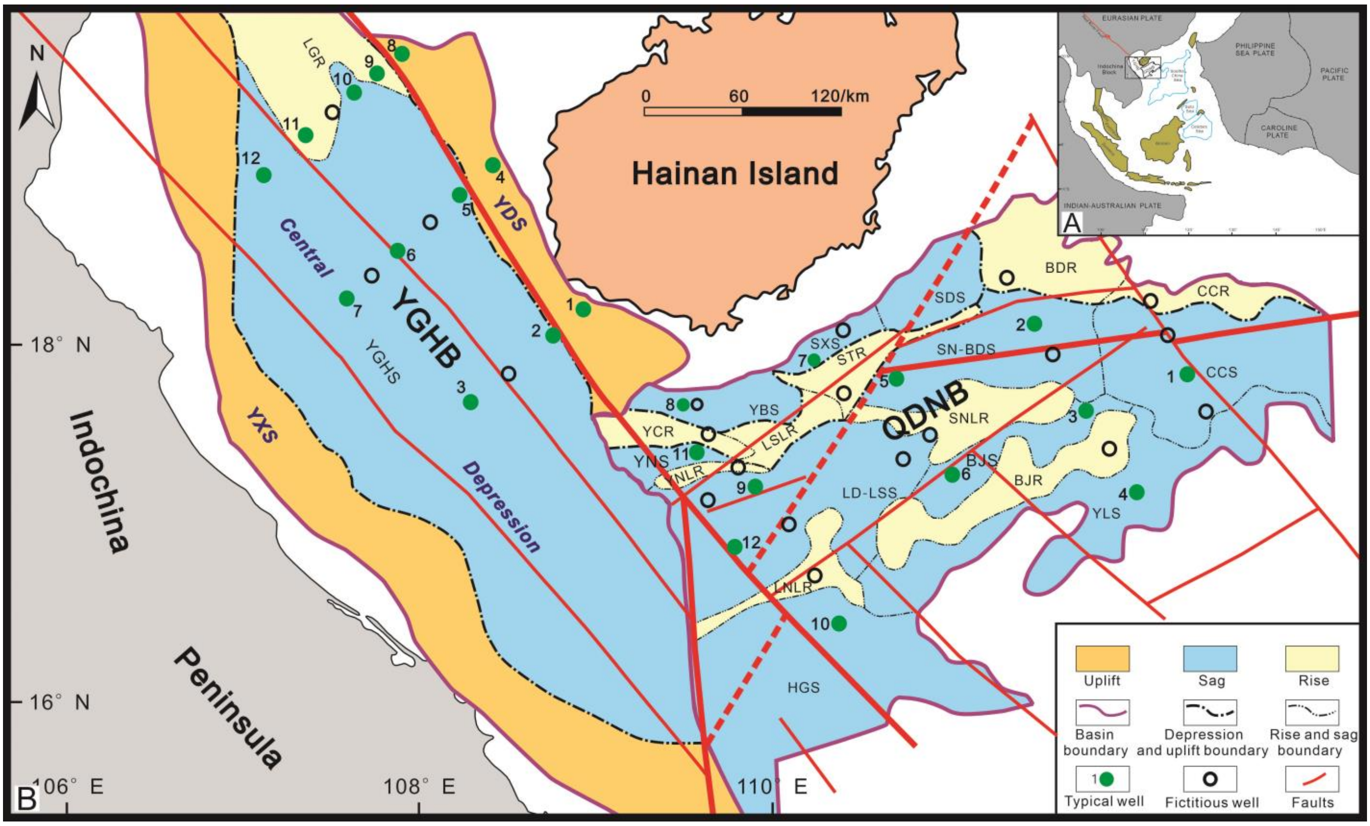

Figure 10. The relationship between the subsidence and basement faults. The abbreviations in this figure are the same as in Figure 1. (The map was modified according to Zhu et al. [19]. The faults are according to Lu et al. [47].)

The major faults significantly affected the subsidence in the two basins (Figure 10). For example, in the QDNB, the areas near the major faults were the subsidence areas in most of the periods of the basin's evolution, including the Changchang sag, Songnan Baodao sag, western Ledonglingshui sag, and Huaguang sag (wells 1, 2, 5, 9, 12, and 10 in Figures 3 and 10). In particular, the western Ledonglingshui sag was always a subsidence area, with a high subsidence rate because of the lithosphere fault that crosses it. In contrast, the areas farther away from the fault were the areas where the non-depocenters were distributed in most of the periods of the basin's evolution, such as the Yongle and Yabei sags (wells 4 and 8 in Figures 3 and 10). The subsidence in the YGHB was closely related to the strike-slip motion of the Red River Fault (Figures 9 and 10). The depocenters had been primarily distributed in the western part of the YGHB in the early period, which matched the left-lateral strike-slip movement of the Red River Fault. However, it shifted to the eastern part of the basin in the Pliocene due to the onset of the dextral strike-slip movement of the Red River Fault (Figures 4 and 10). Furthermore, the depocenters had continuously migrated from northwest to southeast with the southeastward propagation of the Red River Fault and the southeastward transportation of the sediment source. The faults had a significant influence on the subsidence in both basins, which resulted in spatiotemporal variations in the subsidence in the same basin.

6. Conclusions

The main conclusions of this study were as follows.

First, the differences in the subsidence characteristics of the QDNB and the YGHB were distinct, including the subsidence rates, the migrations of the depocenters, and the changes in the ranges of the subsidence.

Second, the changes in the holistic subsidence in both the QDNB and the YGHB occurred in episodes. In the QDNB, the holistic subsidence process could be divided into three episodes, according to the subsidence features. The first episode occurred in the Eocene; the second episode occurred from the Oligocene to the Middle Miocene; and the third episode occurred from the Late Miocene to the Quaternary. The variations in the holistic subsidence rate exhibited wavelike characteristics, with two peaks in the Late Oligocene and Pliocene. In the YGHB, the holistic subsidence process could also be divided into three episodes. The first episode occurred from the Late Miocene to the Early Miocene; the second episode occurred in the Middle and Late Miocene; and the third episode occurred from the Pliocene to the Quaternary. The changes in the holistic subsidence exhibited a distinct wavelike shape, with three crests and troughs, which was a typical subsidence feature of strike-slip basins.

Third, the dynamic variations were the primary factor controlling the differences in the subsidence of the QDNB and the YGHB. The variations in the subsidence characteristics matched the three main geological processes that occurred during this period. The variations in the subsidence in these two basins were obvious before the Pliocene. In the QDNB, the subsidence characteristics were primarily controlled by the variations in the flow of the mantle material under the South China Block in the Eocene and by the spreading of the SCS from the Oligocene to the Miocene. In the YGHB, the subsidence characteristics were chiefly controlled by the combined effects of the uplift of the Tibetan Plateau and the strike-slip motion of the Red River Fault before the Early Miocene and by the strike-slip motion of the Red River Fault from the Middle Miocene to the Late Miocene. Since the Pliocene, the changes in the subsidence in these two basins have been synchronous, and they have primarily been affected by the dextral strike-slip motion of the Red River Fault.

Finally, the major faults also affected the subsidence characteristics, and they induced the spatiotemporal variations in the subsidence within the same basin.

Author Contributions: Conceptualization, M.M. and J.Q.; methodology, H.P., M.M. and J.Q.; software, M.M. and J.M.; validation, H.P. and Q.S.; formal analysis, M.M.; investigation, Q.S.; resources, M.M. and Q.S.; data curation, L.L.; writing—original draft preparation, M.M.; writing—review and editing, M.M., J.Q., M.B., J.M. and L.L.; visualization, J.M.; supervision, Q.Z. and M.M.; project administration, M.M.; funding acquisition, J.Q. All authors have read and agreed to the published version of the manuscript.

Funding: This research was funded by the National Natural Science Foundation of China, grant number 41572202; and the Master's Degree Construction Project of Geological Resources and Geological Engineering of Qinghai University in 2023, grant number 41250103.

Data Availability Statement: The raw data supporting the conclusions of this article will be made available by the authors, without undue reservation.

Acknowledgments: The authors are thankful for the guidance of Qing Liu and Sen Feng in programming.

Conflicts of Interest: The authors declare no conflict of interest.

References

1. Hall, R.; Blundell, D.J. Tectonic evolution of SE Asia: Introduction. In *Tectonic Evolution of Southeast Asia*; Hall, R., Blundell, D.J., Eds.; Geological Society Special Publication: London, UK, 1996; Volume 106, pp. 353–431. [CrossRef]
2. Karig, D.E. Origin and Development of Marginal Basins in the Western Pacific. *J. Geophys. Res.* **1971**, *76*, 2542–2561. [CrossRef]
3. Tapponnier, P.; Molnar, P. Slip-line field theory and large-scale continental tectonics. *Nature* **1976**, *264*, 319–324. [CrossRef]
4. Leloup, P.H.; Amaud, N.; Lacassin, R.; Kienast, J.R.; Harrison, T.M.; Phan Trong, T.T.; Replumaz, A.; Tapponnier, P. New constraints on the structure, thermochronology, and timing of the Ailao Shan-Red River shear zone, SE Asia. *J. Geophys. Res.* **2001**, *106*, 6683–6732. [CrossRef]

5. Xie, X.; Müller, R.D.; Li, S.; Gong, Z.; Steinberger, B. Origin of anomalous subsidence along the Northern South China Sea margin and its relationship to dynamic topography. *Mar. Pet. Geol.* **2006**, *23*, 745–765. [CrossRef]
6. Hall, R.; Hattum, M.W.A.V.; Spakman, W. Impact of India–Asia collision on SE Asia. the record in Borneo. *Tectonophysics* **2008**, *451*, 366–389. [CrossRef]
7. Chen, G. The marginal extensional belt of East Asia Continent-investigating the origin of a discrete continental margin. *Geotecton. Metallog.* **1997**, *21*, 285–293. (In Chinese with English Abstract) [CrossRef]
8. Xia, B.; Zhang, Y.; Cui, X.J.; Liu, B.M.; Xie, J.H.; Zhang, S.L.; Lin, G. Understanding of the geological and geodynamic controls on the formation of the South China Sea. A numerical modelling approach. *J. Geodyn.* **2006**, *42*, 63–84. [CrossRef]
9. Xia, B.; Cui, X.; Xie, J.; Wang, R. Thinking about the dynamics mechanism study on formation and evolution of the South China Sea. *Geotecton. Metallog.* **2004**, *28*, 221–227 (In Chinese with English Abstract) [CrossRef]
10. Ma, M.; Liu, C.; Qi, J.; Zhang, D.; Zhang, S.; Wang, J.; Miao, Q. Cenozoic subsidence history of the Pearl River Mouth Basin, northern South China Sea. *Geol. J.* **2020**, *55*, 750–770. [CrossRef]
11. Liao, F.; Wu, X.; Huang, S. Geochemical Characteristics of Natural Gas in the Yinggehai-Qiongdongnan Basin, South China Sea. *Energy Explor. Exploit.* **2010**, *28*, 1–12. [CrossRef]
12. Zhang, Y.; Zhang, L.; Mi, L.; Lu, X.; Wu, S.; Tang, L.; Zhou, J.; Xiong, X.; Zhu, J. Quantitative Analysis of Cenozoic Extension in the Qiongdongnan Basin, South China Sea: Insight on Tectonic Control for Hydrocarbon Reservoir Accumulation and Formation. *Energies* **2022**, *15*, 4011. [CrossRef]
13. China Institute of International Studies. Available online: https://www.ciis.org.cn/english/COMMENTARIES/202007/t20200715_2762.html (accessed on 11 May 2015).
14. Huang, B.; Xiao, X.; Li, X. Geochemistry and origins of natural gases in the Yinggehai and Qiongdongnan basins, offshore South China Sea. *Org. Geochem.* **2003**, *34*, 1009–1025. [CrossRef]
15. Zhao, Z.; Sun, Z.; Sun, L.; Wang, Z.; Sun, Z. Cenozoic tectonic subsidence in the Qiongdongnan Basin, northern South China Sea. *Basin Res.* **2016**, *30*, 269–288. [CrossRef]
16. Li, X.; Fairweather, L.; Wu, S.; Ren, J.; Zhang, H.; Quan, X.; Jiang, T.; Zhang, C.; Su, M.; He, Y.; et al. Morphology, sedimentary features and evolution of a large palaeo submarine canyon in Qiongdongnan basin, Northern South China Sea. *J. Asian Earth Sci.* **2013**, *62*, 685–696. [CrossRef]
17. Cao, L.; Jiang, T.; Wang, Z.; Zhang, Y.; Sun, H. Provenance of Upper Miocene sediments in the Yinggehai and Qiongdongnan basins, northwestern South China Sea. Evidence from REE, heavy minerals and zircon U–Pb ages. *Mar. Geol.* **2015**, *361*, 136–146. [CrossRef]
18. Shi, X.; Burov, E.; Leroy, S.; Qiu, X.; Xia, B. Intrusion and its implication for subsidence. A case from the Baiyun Sag, on the northern margin of the South China Sea. *Tectonophysics* **2005**, *407*, 117–134. [CrossRef]
19. Zhu, W.; Mi, L. *Atlas of Oil and Gas Basins, China Sea*; Petroleum Industry Press: Beijing, China, 2010; pp. 478–480. (In Chinese)
20. All China Commission of Stratigraphy. *The Instruction of China Regional Stratigraphy (Geological Time Scale) Chart*; Geological Publishing House: Beijing, China, 2002; pp. 235–237. (In Chinese)
21. Wang, X.; Chen, X. *Stratigraphy Division and Correlation of Each Geological Period in China*; Geological Publishing House: Beijing, China, 2005; pp. 278–283. (In Chinese)
22. Chen, Y.; Wang, Z.; Huang, Z. *The Pandect of Stratigraphical of China*; Geological Publishing House: Beijing, China, 2009; p. 557. (In Chinese)
23. Liu, X.; Xie, J.; Zhang, H.; He, W. Chronostratigraphy of planktonic foraminifera in the Yinggehai-Qiongdongnan Basin. *Acta Micropalaeontoligical Sin.* **2009**, *26*, 181–192. (In Chinese with English Abstract)
24. Gao, H.; Du, D.; Zhong, G. Quantitative simulation of subsidence history and analysis of Pearl River Mouth Basin in South China Sea. *Res. Geol. South China Sea* **2006**, *13*, 11–20. (In Chinese with English Abstract)
25. Athy, L.F. Density, Porosity, and Compaction of Sedimentary Rocks. *AAPG Bull.* **1930**, *14*, 1–24. [CrossRef]
26. Airy, G.B. On the Computation of the Effect of the Attraction of Mountain-Masses, as Disturbing the Apparent Astronomical Latitude of Stations in Geodetic Surveys. *Philos. Trans. R. Soc. Lond.* **1855**, *145*, 101–104. [CrossRef]
27. Steckler, M.S.; Watts, A.B. Subsidence of the Atlantic-type continental margin off New York. *Earth Planet. Sci. Lett.* **1978**, *41*, 1–13. [CrossRef]
28. Mckenzie, D.P. Some remarks on the development of sedimentary basins. *Earth Planet. Sci. Lett.* **1978**, *40*, 25–32. [CrossRef]
29. Sclater, J.G.; Christie, P.A.F. Continental stretching. An explanation of the Post-Mid-Cretaceous subsidence of the central North Sea Basin. *J. Geophys. Res. Solid Earth* **1980**, *85*, 3711–3739. [CrossRef]
30. Allen, P.A.; Allen, J.R. *Basin Analysis. Principles and Applications to Petroleum Play Assessment*, 3rd ed.; John Wiley & Sons Ltd.: Chichester, UK, 2013; p. 523.
31. Madon, M.B.; Watts, A.B. Gravity anomalies, subsidence history and the tectonic evolution of the Malay and Penyu Basins (offshore Peninsular Malaysia). *Basin Res.* **1998**, *10*, 375–392. [CrossRef]
32. Watts, A.B.; Steckler, M.S. Subsidence and eustasy at the continental margin of eastern North America. In *Deep Drilling Results in the Atlantic Ocean. Continental Margings and Paleoenviroment*; Maurice Ewing Symposium Series; Talwani, M., Hay, W., Ryan, W.B.F., Eds.; American Geophysical Union: Washington, DC, USA, 1979; Volume 3, pp. 218–234.
33. Haq, B.U.; Hardenbol, J.; Vail, P.R. Chronology of fluctuating sea levels since the Triassic. *Science* **1987**, *235*, 1156–1167. [CrossRef] [PubMed]
34. Kominz, M.A.; Browning, J.V.; Miller, K.G.; Sugarman, P.J.; Mizintseva, S.; Scotese, C.R. Late Cretaceous to Miocene sea-level estimates from the New Jersey and Delaware coastal plain coreholes. An error analysis. *Basin Res.* **2008**, *20*, 211–226. [CrossRef]
35. Yin, A.; Harrison, T.M. Geologic Evolution of the Himalayan-Tibetan Orogen. *Annu. Rev. Earth Planet. Sci.* **2000**, *28*, 211–280. [CrossRef]

36. Northrup, C.J.; Royden, L.H.; Burchfiel, B.C. Motion of the Pacific plate relative to Eurasia and its potential relation to Cenozoic extension along the eastern margin of Eurasia. *Geology* **1995**, *23*, 719–722. [CrossRef]
37. Yao, B. The Tectonic evolution and sedimentary basins of South China Sea in Cenozoic. *Geol. Res. South China Sea* **1998**, *10*, 1–17. (In Chinese with English Abstract)
38. Briais, A.; Patriat, P.; Tapponnier, P. Updated interpretation of magnetic anomalies and seafloor spreading stages in the south China Sea. Implications for the Tertiary tectonics of Southeast Asia. *J. Geophys. Res. Solid Earth* **1993**, *98*, 6299–6328. [CrossRef]
39. Clift, P.D.; Sun, Z. The sedimentary and tectonic evolution of the Yinggehai-Song Hong basin and the southern Hainan margin, South China Sea. Implications for Tibetan uplift and monsoon intensification. *J. Geophys. Res. Solid Earth* **2006**, *111*, 1–28. [CrossRef]
40. Dupré, S.; Bertotti, G.; Cloetingh, S. Tectonic history along the South Gabon Basin. Anomalous early post-rift subsidence. *Mar. Pet. Geol.* **2007**, *24*, 151–172. [CrossRef]
41. Yin, X.; Ren, J.; Lei, C.; Wang, S.; Zhang, J. Post rift rapid subsidence characters in Qiongdongnan Basin, South China Sea. *J. Earth Sci.* **2011**, *22*, 273–279. [CrossRef]
42. Zhong, D.; Ding, L. The discussion of the uplift process of the Tibetan Plateau and its mechanism. *Sci. China (Ser. D)* **1996**, *26*, 289–295. (In Chinese)
43. Sun, Z.; Zhou, D.; Zhong, Z.; Zeng, Z.; Wu, S. Experimental evidence for the dynamics of the formation of the Yinggehai basin, NW South China Sea. *Tectonophysics* **2003**, *372*, 41–58. [CrossRef]
44. Lee, T.Y.; Lawver, L.A. Cenozoic plate reconstruction of Southeast Asia. *Tectonophysics* **1995**, *251*, 85–138. [CrossRef]
45. Coleman, M.; Hodges, K. Evidence for Tibetan plateau uplift before 14 Myr ago from a new minimum age for east-west extension. *Nature* **1995**, *374*, 49–52. [CrossRef]
46. Krishnappan, B.G. Reviewof a Semi-Empirical Modelling Approach for Cohesive Sediment Transport in River Systems. *Water* **2022**, *14*, 256. [CrossRef]
47. Lu, B.; Wang, P.; Zhang, G.; Wang, W. Characteristic of regional fractures in South China Sea and its basement tectonic framework. *Prog. Geophys.* **2015**, *30*, 1544–1553. (In Chinese with English Abstract) [CrossRef]